

## On the Possibilities of Detecting Helium D<sub>3</sub> Line Polarization with Metis

PETR HEINZEL,<sup>1</sup> JIŘI ŠTĚPÁN,<sup>1</sup> ALESSANDRO BEMPORAD,<sup>2</sup> SILVANO FINESCHI,<sup>2</sup> SONJA JEJČIČ,<sup>3,4,1</sup> NICOLAS LABROSSE,<sup>5</sup>  
AND ROBERTO SUSINO<sup>2</sup>

<sup>1</sup>*Astronomical Institute, The Czech Academy of Sciences, 25165 Ondřejov, Czech Republic*

<sup>2</sup>*INAF - Turin Astrophysical Observatory, Via Osservatorio 20, 10025 Pino Torinese, TO, Italy*

<sup>3</sup>*Faculty of Education, University of Ljubljana, Kardeljeva ploščad 16, 1000 Ljubljana, Slovenia*

<sup>4</sup>*Faculty of Mathematics and Physics, University of Ljubljana, Jadranska 19, 1000 Ljubljana, Slovenia*

<sup>5</sup>*SUPA, School of Physics & Astronomy, University of Glasgow, Glasgow, G12 8QQ, UK*

(Received Month DD, 2020; Revised Month DD, 2020; Accepted Month DD, 2020)

Submitted to ApJ

### ABSTRACT

Space coronagraph Metis on board of the Solar Orbiter offers us new capabilities for studying eruptive prominences and coronal mass ejections (CME). Its two spectral channels, hydrogen L $\alpha$  and visible-light (VL) will provide, for the first time, co-aligned and co-temporal images to study dynamics and plasma properties of CMEs. Moreover, with the VL channel (580 - 640 nm) we find an exciting possibility to detect the helium D<sub>3</sub> line (587.73 nm) and its linear polarization. The aim of this study is to predict the diagnostics potential of this line regarding the CME thermal and magnetic structure. For a grid of models we first compute the intensity of the D<sub>3</sub> line together with VL continuum intensity due to Thomson scattering on core electrons. We show that the Metis VL channel will detect a mixture of both, with predominance of the helium emission at intermediate temperatures between 30 - 50,000 K. Then we use the code HAZEL to compute the degree of linear polarization detectable in the VL channel. This is a mixture of D<sub>3</sub> scattering polarization and continuum polarization. The former one is lowered in the presence of a magnetic field and the polarization axis is rotated (Hanle effect). Metis has the capability of measuring  $Q/I$  and  $U/I$  polarization degrees and we show their dependence on temperature and magnetic field. At  $T=30,000$  K we find a significant lowering of  $Q/I$  which is due to strongly enhanced D<sub>3</sub> line emission, while depolarization at 10 G amounts roughly to 10 %.

### 1. INTRODUCTION

Magnetic-field measurements in cool coronal structures like prominences, coronal rain or CMEs represent a challenging problem. In case of quiescent prominences, several attempts were made to determine the supporting magnetic fields using the spectro-polarimetry - for a review see López Ariste (2015). Prominences are low-density media and thus the scattering of the incident solar radiation determines their emissivity. Their illumination by the solar disk is largely anisotropic which leads to a linear polarization of the scattered radiation. The presence of a magnetic field, which is rather weak in prominences, then causes a lowering of the polarization degree and rotation of the polarization plane (Hanle effect, see Landi Degl'Innocenti & Landolfi (2004)). Typical range of the magnetic-field strength in quiescent prominences is around 10 G, but fields as high as tens of G have also been reported (López Ariste 2015). Recently, much stronger field was detected in post-flare loops, earlier called loop prominences and nowadays identified with a coronal rain. However, in case of flare loops with the field strength of a few hundreds of Gauss, the polarization is due to Zeeman effect and the weak-field approximation was used to determine the field strength (Kuridze et al. 2019). Another class of relatively cool coronal structures is represented by cores of Coronal Mass Ejections (CME), where the kinetic temperatures are on the order  $10^4$  to  $10^5$  K or more (see e.g. Heinzl et al. (2016) and Jejčič et al. (2018)). In these structures, however, the magnetic field was never measured. This is related to the fact that CMEs

are mostly observed from space, using coronagraphs in visible light (e.g. LASCO on board SOHO and COR1 and COR2 on board STEREO missions) or with the UV spectrograph like UVCS on board SOHO. Nevertheless, there are no spectro-polarimeters attached to space coronagraphs capable of measuring the linear polarization in spectral lines emitted by prominence-like structures including CME cores. A giant coronagraph ASPIICS on board the ESA's Proba-3 formation-flight mission (Lamy et al. 2017) will detect the helium D<sub>3</sub> line at 587.73 nm (vacuum wavelength), but only the integrated intensity and no polarization. D<sub>3</sub> line polarization in prominence-like structures was studied in many cases, both theoretically as well as observationally (see López Ariste (2015) and, therefore, some attempts were made to include D<sub>3</sub> polarization measurements in the concept of ASPIICS. But due to different reasons the final set-up will provide polarization detection only in the broad-band visible channel important for determinations of the electron density.

With the launch of the ESA-NASA Solar Orbiter mission, we find an exciting possibility to detect the D<sub>3</sub> line polarization in eruptive prominences and CMEs, using the Metis coronagraph (for Metis description see Antonucci et al. (2019)). This is because the visible-light (VL) continuum channel of Metis in the range between 580 - 640 nm contains the D<sub>3</sub> line at its wavelength edge, still well detectable, and this channel will provide the polarization measurements. Note that Metis has another imaging capability in the hydrogen Lyman  $\alpha$  line, which will provide important diagnostics of the CMEs and coronal plasmas. The situation with Metis VL channel is similar to that of SOHO/LASCO-C2, where the orange VL channel also contains the helium D<sub>3</sub> line. Quite recently, Floyd & Lamy (2019) analyzed several CMEs detected in the orange channel of LASCO-C2 and they discuss apparent signatures of the D<sub>3</sub> polarization. On the other hand, Dolei et al. (2014) were able to extract the H $\alpha$  line polarization in a CME combining STEREO-COR1 and LASCO-C2 observations and they suggested that this could be used to determine the magnetic field in CMEs.

Our idea is to use the Metis VL channel to detect the D<sub>3</sub> polarization in CMEs and possibly to measure their magnetic fields. The main difficulty is that the expected line polarization is mixed with the linear continuum polarization which is due to Thomson scattering on CME electrons. In this paper we estimate theoretically the amount of D<sub>3</sub> line polarization under typical CME conditions and compare it with the respective continuum component. Then we discuss possibilities of the magnetic-field determination based on Metis observations.

## 2. MODELS OF ERUPTIVE PROMINENCES AND CMES

For the purpose of this exploratory work we use the prominence-CME models as described by Jejčič et al. (2018) who studied the capabilities of the narrow-band D<sub>3</sub> filter for ASPIICS. Since the temperatures in those models range from 8,000 K up to 10<sup>5</sup> K, the models we select here can represent cool erupting prominence plasma as well as hot cores of CMEs (Heinzl et al. 2016). The electron densities  $n_e$  are first computed with the hydrogen code and then used to synthesize the helium lines as in Labrosse & Gouttebroze (2001) and Labrosse & Gouttebroze (2004). Note that we neglect here the effect of potentially large CME velocities on the electron density, an aspect to be considered in a future modeling. Such velocities, however, do not affect the formation of the D<sub>3</sub> line because the prominence is illuminated by a continuum radiation, i.e. no Doppler brightening effect takes place. D<sub>3</sub> line-center optical thickness  $\tau_0$  is the input parameter for our polarized radiative-transfer modeling. We need to know the relation between  $\tau_0$  and  $n_e$  in order to consistently evaluate the D<sub>3</sub> and VL emissions which enter the Metis filter passband. From a grid of 90 models computed in Jejčič et al. (2018) we selected 20 representative ones as shown in Table 1. We choose two heights above the solar surface, and namely 800 Mm with geometrical dilution factor  $W=0.058$  and 1600 Mm with  $W=0.024$ , which correspond to 2.15 and 3.30 solar radii measured from the disk center, respectively, in the range covered by Metis at its closest approach to the Sun. The dilution factor  $W$  substantially decreases with height which lowers the amount of exciting radiation but simultaneously increases its anisotropy. For the effective geometrical thickness  $D$  we choose 5 Mm which, together with a low filling factor (Susino et al. 2018), represents plausible sizes of CME cores. The selected gas pressures give the hydrogen ionization comparable to situations in eruptive prominences and hot CMEs. Similarly as in Jejčič et al. (2018) we increase the microturbulent velocity with increasing temperature (see the case or a CME flux-rope in Jejčič et al. (2017)).

## 3. HELIUM D<sub>3</sub> LINE FORMATION IN PROMINENCES AND CMES

Formation of the helium D<sub>3</sub> line under non-LTE conditions (i.e. departures from the Local Thermodynamic Equilibrium) is a complex multilevel radiative-transfer problem. In case of solar prominences it was treated in detail by Heasley et al. (1974) and later on by Labrosse & Gouttebroze (2001) and Labrosse & Gouttebroze (2004) (see also

**Table 1.** Grid of models used for synthesis of polarized radiation in D<sub>3</sub> line and VL.

model	$h$ km	$T$ K	$p$ dyn cm <sup>-2</sup>	$D$ km	$v_t$ km s <sup>-1</sup>	$n_e$ cm <sup>-3</sup>	$E(D_3)$ cgs	$\tau_0(D_3)$	$E(VL)$ cgs
1	800000	8,000	0.05	5000	5	3.83+9	44.2	8.4-4	90.3
2	800000	15,000	0.05	5000	5	1.15+10	34.9	5.2-4	271.0
3	800000	30,000	0.05	5000	15	6.29+9	885.0	6.7-3	148.2
4	800000	50,000	0.05	5000	15	3.78+9	176.9	1.2-3	89.1
5	800000	100,000	0.05	5000	20	1.89+9	2.8	1.6-5	44.5
6	800000	8,000	0.1	5000	5	8.35+9	35.8	6.8-4	196.8
7	800000	15,000	0.1	5000	5	2.34+10	66.1	9.5-4	551.5
8	800000	30,000	0.1	5000	15	1.26+10	2244.4	1.6-2	297.0
9	800000	50,000	0.1	5000	15	7.56+9	439.8	2.7-3	178.2
10	800000	100,000	0.1	5000	20	3.78+9	6.9	3.6-5	89.1
11	1600000	8,000	0.05	5000	5	1.75+9	7.5	3.3-4	16.5
12	1600000	15,000	0.05	5000	5	1.13+10	6.9	2.0-4	106.5
13	1600000	30,000	0.05	5000	15	6.29+9	290.4	3.7-3	59.3
14	1600000	50,000	0.05	5000	15	3.78+9	57.9	6.2-4	35.6
15	1600000	100,000	0.05	5000	20	1.89+9	0.9	8.2-6	17.8
16	1600000	8,000	0.1	5000	5	4.07+9	6.1	2.6-4	38.4
17	1600000	15,000	0.1	5000	5	2.31+10	20.3	5.3-4	217.7
18	1600000	30,000	0.1	5000	15	1.26+10	850.9	8.7-3	118.8
19	1600000	50,000	0.1	5000	15	7.56+9	170.0	1.4-3	71.3
20	1600000	100,000	0.1	5000	20	3.78+9	2.6	1.8-5	35.6

reviews by [Labrosse et al. \(2010\)](#) and [Labrosse \(2015\)](#)). The latter authors used a multi-level He I model atom depicted in Figure 1 and solving the multi-ion statistical equilibrium equations they obtained the ionization structure, level populations and optical properties of the helium. Here we will focus only on the formation of the D<sub>3</sub> line, which can be approximately separated into two problems: the excitation of level 9 from which the optically-thin D<sub>3</sub> emission arises, and population of the lower level 4 which determines the optical thickness  $\tau_0$  of the D<sub>3</sub> line (see Table 1). While the first aspect can be treated as a two-level atom problem, the second one is a complex multilevel-multiion non-LTE problem. Optical thickness  $\tau_0$  and integrated intensity of D<sub>3</sub> result from the helium multilevel modeling as described in [Labrosse & Gouttebroze \(2001\)](#) (note that the helium non-LTE code uses as input the electron density previously computed with the hydrogen code). These quantities are shown in Table 1, together with the visible-light (VL) intensity integrated over the Metis VL passband 580 - 640 nm. VL emission is due to Thomson scattering on prominence or CME electrons and was computed using the limb-darkened incident continuum radiation from the solar disk (e.g. [Cox \(2000\)](#)). We can see from Table 1 that even using this wide-band Metis filter, the D<sub>3</sub> line intensity is not negligible in comparison to VL intensity and namely for higher temperatures around 30 - 50,000 K the D<sub>3</sub> intensity dominates the VL one. This means that we may expect a non-negligible contribution of D<sub>3</sub> to total polarization signal from Metis filter. This is also consistent with the conclusions of [Floyd & Lamy \(2019\)](#) who found CME signatures of the D<sub>3</sub> emission within even wider (100 nm) broad-band orange filter of LASCO-C2 coronagraph. First question arises how the upper level 9 of the D<sub>3</sub> transition is excited. In [Jejčić et al. \(2017\)](#) the authors suggest that much brighter D<sub>3</sub> at  $T=30,000$  K can be due to stronger collisional excitations at higher temperatures. This of course would produce a non-polarized emission, i.e. the scattering term will be negligible compared to collisional one in the line source function. We know that collisions, both inelastic as well as elastic, are negligible at typical prominence temperatures below say 10,000 K, but how it will be at much higher temperatures found in CME cores? In order to answer this critical question, we made two calculations. First, we quantitatively compared the collisional excitation rates to upward radiative ones (i.e. those leading to scattering). Their ratio is

$$x = \frac{n_e C_{49}}{B_{49} I_0 W}, \quad (1)$$

where  $B_{49}$  is the Einstein coefficient for absorption,  $I_0$  the disk-center continuum intensity at the  $D_3$  wavelength and  $W$  the geometrical dilution factor (in this estimate we neglect the continuum limb darkening).  $C_{49}$  is the collisional rate depending on temperature. We found that for all models considered here this ratio is quite small, the radiative rates are several orders of magnitude larger than the collisional ones, even at high temperatures. This is a good news since the line source function in this two-level model is dominated by scattering. We also found negligible collisional rates for transition between levels 2 and 4 which means that the level 4 is populated by radiative excitation and thus is polarized (see the next section).

The other independent calculation shows that actually all  $D_3$  line intensities from Table 1 result from almost identical line source function which is dominated by scattering. For the line integrated intensity we can simply write

$$E = \sqrt{\pi} \Delta\lambda_D S \tau_0, \quad (2)$$

where  $\Delta\lambda_D$  is the line Doppler width and  $S$  is the line source function. Using  $E$ ,  $\Delta\lambda_D$  and  $\tau_0$  according to Table 1, we find that resulting source function  $S$  is almost identical for all models. This then means that also at higher temperatures it must be dominated by scattering.

However, there is still a question why  $D_3$  brightness is so large at temperatures around 30,000 K and this is the other aspect of the  $D_3$  line formation problem. Looking at Eq. 2 we see that, for a fixed  $S$ ,  $E$  varies due to changes of  $\Delta\lambda_D$  and  $\tau_0$ . However, the product  $\Delta\lambda_D \times \tau_0$  is directly proportional to number density of He I atoms in level 4, i.e. the level 4 population. Since the level 4 is mainly populated by radiative excitations from level 2, i.e. the scattering in 1083 nm line (collisional excitation is again negligible at low densities), the temperature dependence of  $\tau_0(D_3)$  must follow that of the 2nd level population. It is generally known that this particular triplet state is populated by recombinations (radiative and di-electronic) from He II ion. Therefore, it must depend on the ionization rate from He I to He II. If this population should be dependent on temperature, the collisional ionization of He I from its ground state must dominate over the radiative one. We thus computed these two rates. The radiative (photoionization) rate was estimated using the incident EUV ionizing radiation below 50.4 nm and the collisional ionization rates were computed according to [Mihalas & Stone \(1968\)](#). Very interestingly, around  $T=30,000$  K, the collisional ionization is already dominant over the photoionization by almost one order of magnitude while at low temperatures it is quite negligible. We may thus expect a significant temperature-dependent increase of He II density and thus also of population of the triplet ground state 2 due to photo-recombinations. However, for much higher temperatures reaching  $10^5$  K,  $\tau_0(D_3)$  will substantially decrease due to strong ionization of helium (see Table 1). In summary, we see that  $E(D_3)$  is varying with temperature due to He I collisional ionization and subsequent photo-recombinations, but the line source function is completely dominated by scattering. Note that a slight difference from such a source function at high temperatures is probably due to recombinations directly to level 4.

#### 4. VISIBLE-LIGHT AND $D_3$ SCATTERING POLARIZATION

##### 4.1. Visible-light component

For the sake of simplicity, we consider a simple scattering geometry shown in Figure 2. The plasma located in the plane of the sky at the height  $h$  above the solar surface is illuminated by an anisotropic radiation from the underlying solar photosphere. We assume the illumination is due to an unpolarized solar continuum radiation in the whole spectral interval of the VL filter. Due to the limb darkening effect, the incident intensity  $I^{\text{inc}}(\lambda, \theta)$  at wavelength  $\lambda$  depends on the incident angle  $\theta$ . In our calculations, we use interpolated data from [Cox \(2000\)](#) for  $I^{\text{inc}}(\lambda, \theta)$ .

The VL continuum emission is predominantly due to the Thomson scattering. In order to calculate the intensity and linear polarization of the scattered radiation at a given height and wavelength, two components of the radiation field tensor need to be considered, namely  $J_0^0$  that corresponds to the common mean radiation field intensity  $J$ , and  $J_0^2$  that quantifies anisotropy of the incident field:

$$J_0^0(\lambda) = \frac{1}{2} \int_{-1}^1 I^{\text{inc}}(\lambda, \mu) d\mu, \quad (3)$$

$$J_0^2(\lambda) = \frac{1}{4\sqrt{2}} \int_{-1}^1 (3\mu^2 - 1) I^{\text{inc}}(\lambda, \mu) d\mu, \quad (4)$$

where  $\mu = -\cos\theta$  (for more details, see [Landi Degl'Innocenti & Landolfi \(2004\)](#)). In Figure 3, we show the height dependence of these quantities at the wavelength  $\lambda = 600$  nm. Even though these quantities depend on wavelength,

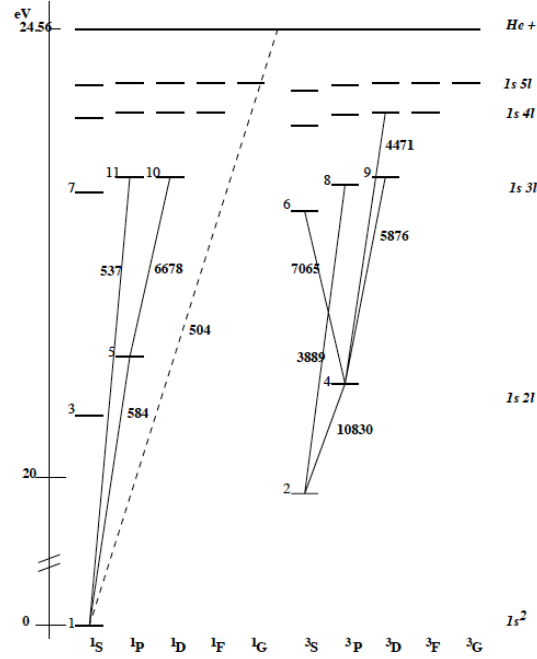


**Figure 1.** Atomic level and transition diagram for He I atom. The wavelengths of line transitions are indicated, the dashed line represents the ionization continuum from the ground state. This line also schematically divides the singlet and triplet states of He I. Here the D<sub>3</sub> line is due to transition between levels 4 and 9.

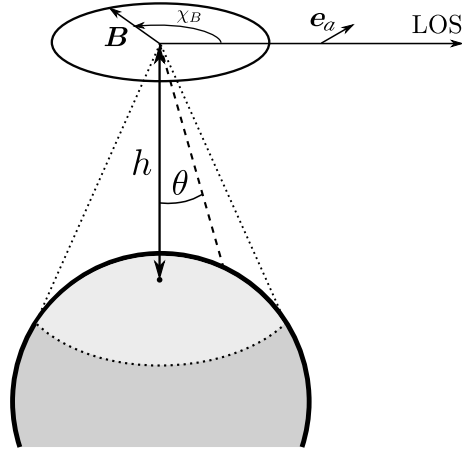


**Figure 2.** Scattering geometry considered in this paper. The plasma is located at the height  $h$  above the solar surface and scatters the incident disk radiation that arrives at the angle  $\theta$  between the local vertical and the direction of illumination. The positive Stokes  $Q$  direction (i.e., the  $\vec{e}_a$  vector) is parallel to the nearest solar limb. The magnetic field vector  $\vec{B}$  is perpendicular to the solar radius and deviates by an angle  $\chi_B$  from the line of sight (LOS) that is chosen to be perpendicular to the local vertical direction.

this dependence is rather weak in the interval of interest (580 — 640 nm). As it follows from the plot, the fractional anisotropy  $J_0^2/J_0^0$  rapidly increases with height and so is the fractional polarization of the emitted VL radiation (see below).

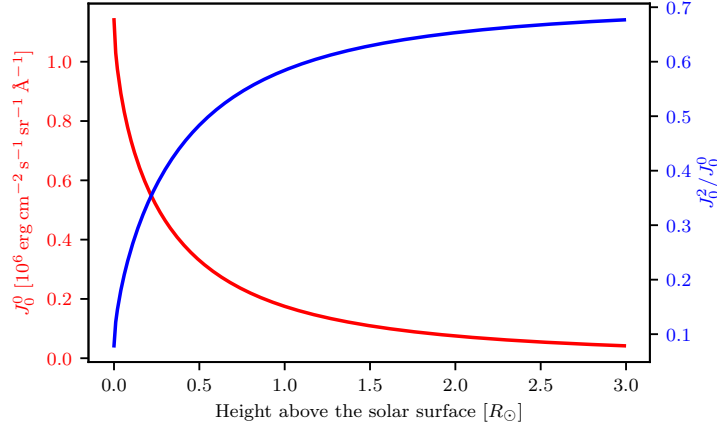


**Figure 3.** Mean intensity ( $J_0^0$ ) and fractional anisotropy ( $J_0^2/J_0^0$ ) as a function of height above the solar surface at the wavelength  $\lambda = 600$  nm.

The continuum optical thickness of the slab of free electrons is independent of wavelength and equal to  $\tau_e = n_e \sigma_T D$ , where  $n_e$  is the electron number density,  $\sigma_T \approx 6.65 \times 10^{-25} \text{ cm}^{-2}$  is the Thomson scattering cross-section, and  $D$  is the geometrical thickness of the slab. In the models considered in this paper, we are always in the regime of very small optical thickness,  $\tau_e \ll 1$ . In that case, the scattered continuum intensity (Stokes parameter  $I$ ) and linear polarization (Stokes parameter  $Q$ ) in the geometrical configuration of Figure 2 are equal to the respective Stokes source functions  $S_I$  and  $S_Q$  multiplied by the optical thickness of the medium. The source functions of the Stokes parameters can be easily derived (e.g., Trujillo Bueno & Shchukina 2009) and the expressions for the emergent Stokes parameters read

$$I(\lambda) = \tau_e S_I(\lambda) = \tau_e J_0^0(\lambda) \left[ 1 - \frac{1}{2\sqrt{2}} \frac{J_0^2(\lambda)}{J_0^0(\lambda)} \right], \quad (5)$$

$$Q(\lambda) = \tau_e S_Q(\lambda) = \tau_e \frac{3}{2\sqrt{2}} J_0^2(\lambda). \quad (6)$$

We note that at heights above  $h \approx 0.1 R_\odot$ , the second term in Eq. (5) is not negligible (see Figure 3) and since  $J_0^2 > 0$ , the emitted intensity is lower than one would expect if anisotropy and polarization phenomena were neglected.

Integration of the above expressions over the Metis VL pass-band gives us the observable total emissivities of VL in intensity and linear polarization,

$$E_I = \int I(\lambda) \phi(\lambda) d\lambda, \quad (7)$$

$$E_Q = \int Q(\lambda) \phi(\lambda) d\lambda, \quad (8)$$

where  $\phi(\lambda)$  is a normalized spectral sensitivity of the instrument. For the sake of simplicity, we consider  $\phi(\lambda) = 1$  in the range between 580 - 640 nm (see Antonucci et al. (2019)).

The linear polarization of the VL is parallel to the nearest solar limb, i.e., the Stokes parameter  $U$  and  $E_U = \int U(\lambda) \phi(\lambda) d\lambda$  are equal to zero, and it is insensitive to presence of magnetic field. In contrast to Thomson scattering, the linear polarization of the D<sub>3</sub> line is sensitive to the magnetic fields via the Hanle and Zeeman effects. If the wavelength-integrated signal is contaminated by the photons emitted by the He I atoms, the  $E_I$ ,  $E_Q$ , and  $E_U$  can, in principle, provide information on the magnetic field vector in the slab.

#### 4.2. Spectral line component

As shown by Bommier (1977), once the density of orthohelium is known from the non-LTE calculation, the atomic model sufficient for synthesis of the D<sub>3</sub> line intensity and polarization consists of the terms 2, 4, 6, 8, 9 in Figure 1 with total 11 fine-structure levels. In the low-density plasma of our interest, the depolarizing collisions can be neglected

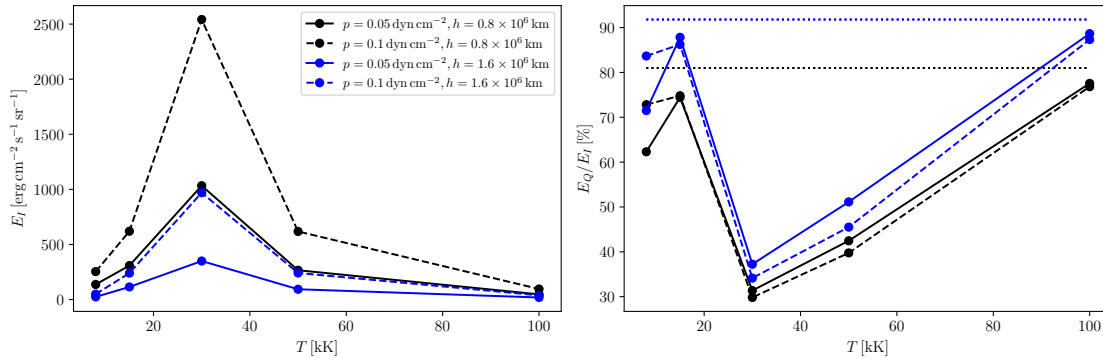


**Figure 4.** Left panel: integrated intensity  $E_I(\text{D}_3+\text{VL})$ . Right panel: integrated linear-polarization degree  $E_Q(\text{D}_3+\text{VL})/E_I(\text{D}_3+\text{VL})$  signal. The signals for two different heights above the solar surface and two different plasma pressures are plotted as functions of kinetic temperature. The horizontal dotted lines in the right panel show the fractional polarization of the VL, neglecting the  $\text{D}_3$  contribution, at the heights  $h = 0.8 \times 10^6$  km (black line) and  $1.6 \times 10^6$  km (blue line).

(Sahal-Brechot et al. 1977). Since the optical thickness of  $\text{D}_3$  (and presumably of the other considered lines) is smaller than one, cf. Table 1, and since the incident photospheric radiation is spectrally flat across the  $\text{D}_3$  line and, to a large extent across the other relevant lines of the model atom, the suitable picture of atomic levels is the multi-term approximation of Sect. 7.6 of Landi Degl’Innocenti & Landolfi (2004) and the discussion in Sect. 13.4 therein.

For the synthesis of the  $\text{D}_3$  line we use the code HAZEL (Asensio Ramos et al. 2008) which is applicable in the regime of our interest, namely in the limit of a constant-property slab. Given the height above the solar disk, magnetic field vector, and optical thickness of the slab obtained from the multi-ion non-LTE solution, we can calculate the line Stokes profiles and normalize the spectrum to the integrated absolute emissivity obtained from the unpolarized non-LTE solution (see Table. 1). HAZEL uses the same five-term model atom as discussed above and takes properly into account the limb darkening effects in all the spectral lines.

At first, we consider the case of non-magnetic plasma ( $B = 0$  G) and we calculate the dependence of the total (VL and  $\text{D}_3$ ) integrated intensity and fractional polarization for different models. The results can be found in Figure 4. We see a significant depolarization effect due to the  $\text{D}_3$  line that is most apparent at intermediate temperatures around 30,000 K. This is closely related to the fact that at these temperatures the  $\text{D}_3$  line is extremely bright, hence both the intensity and fractional polarization signal are dominated by the line instead of the VL (see Table 1). Since fractional polarization of the line is always smaller than polarization of the VL, the presence of the line always leads to depolarization of the total signal (i.e. lowering of the fractional polarization). We note that fractional polarization of the line,  $E_Q(\text{D}_3)/E_I(\text{D}_3)$  is practically insensitive to the model in the range of parameters of Table 1 and it only depends on the height above the solar surface and on the local magnetic field vector. In the following section, we discuss the magnetic sensitivity of the total VL+ $\text{D}_3$  signal.

## 5. MAGNETIC FIELD AND THE HANLE EFFECT

### 5.1. Flux-rope Magnetic Field in CMEs

Measurements of magnetic fields in solar prominences are very difficult (see e.g. review by López Ariste (2015)) and usually require long integration times in order to detect weak polarization signals. To our knowledge, the magnetic field inside erupting prominences has never been measured during the eruption in the expansion phase across the intermediate corona (what will be observed by Metis). However, in a recent paper by Fan et al. (2018) the authors are simulating the appearance of an erupting prominence with the COSMO coronagraph, with the aim to demonstrate the feasibility of magnetic field determination from circular polarization measurements of the Fe XIII line undergoing Zeeman effect. This paper provides the  $B_{\text{LOS}}$  (i.e. the LOS averaged magnetic field) inside an erupting prominence at different times during the eruption. From their Figs. 3, 11, and 15, in the early eruption phase (below 1.4 solar radii from the disk center) one can assume maximum of 5-10 G at the center of the flux rope. For larger altitudes, we have to make some empirical considerations. Assuming that the flux rope is expanding self-similarly, and using a well known empirical relationship between the radial speed  $v_{\text{rad}}$  and the expansion speed  $v_{\text{exp}}$  of a CME,  $v_{\text{rad}} = 0.88v_{\text{exp}}$  (Dal Lago et al. 2003), basically one can assume that  $h_{\text{CME}} = 0.88r_{\text{CME}}$  and the same relationship holding between

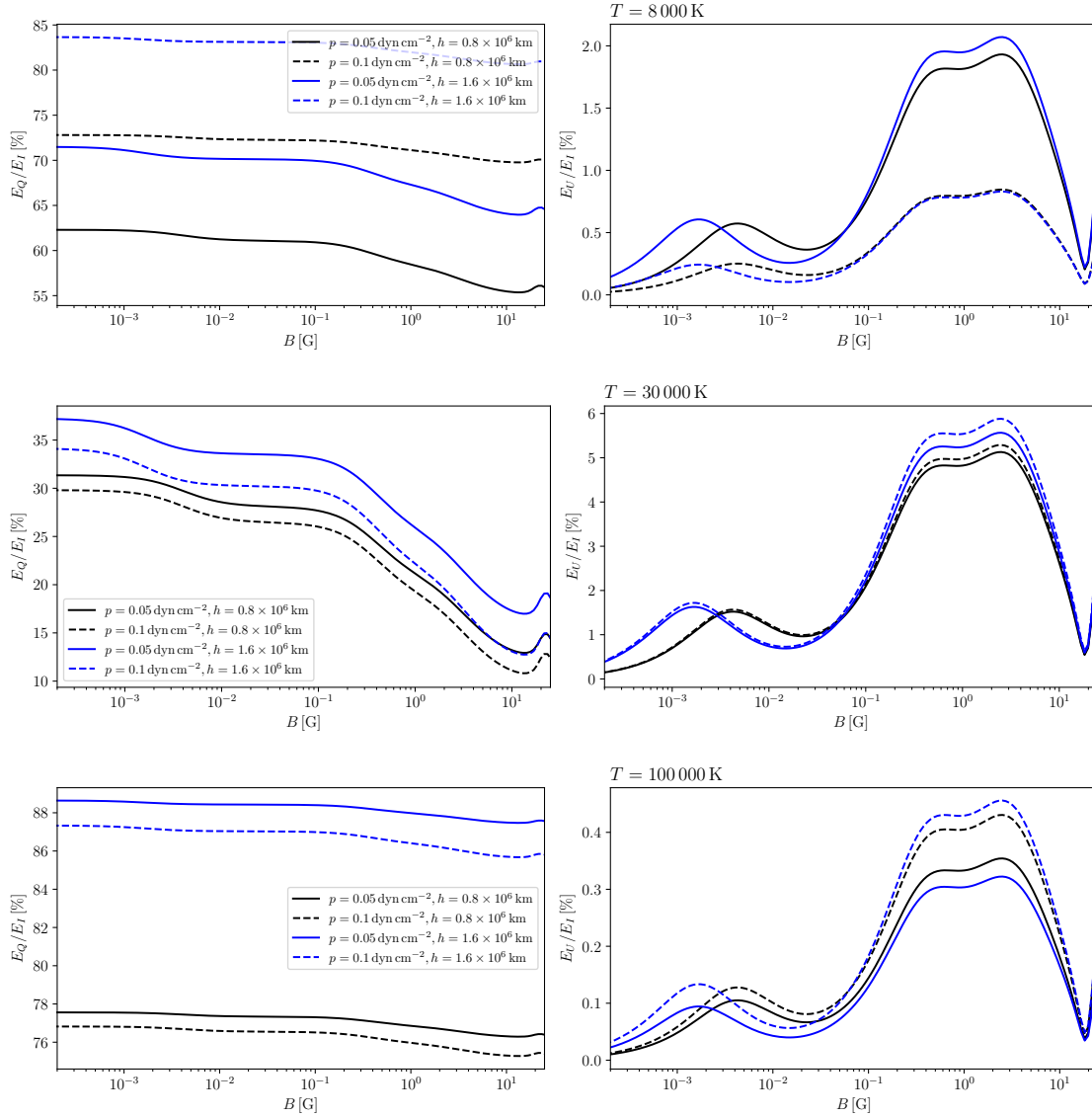


**Figure 5.** Total (i.e., VL and D<sub>3</sub>) fractional polarization signals  $E_Q/E_I$  (left panels) and  $E_U/E_I$  (right panels) for different models as a function of magnetic field intensity. From top to bottom, the panels show models with temperatures 8,000, 30,000, and 100,000 K. The magnetic field is oriented along the LOS ( $\chi_B = 0^\circ$ ).

the altitude of the CME and the radius of the flux-rope. This means that the cross-sectional area  $A_{\text{FR}}$  of the flux rope is going with the CME altitude  $h_{\text{CME}}$  like

$$A_{\text{FR}} = \pi r_{\text{CME}}^2 = \pi (h_{\text{CME}}/0.88)^2 \propto h_{\text{CME}}^2. \quad (9)$$

Now, if we assume the magnetic flux conservation during the expansion, we can write that  $B(0)A_{\text{FR}}(0) = B(h)A_{\text{FR}}(h)$ . Therefore, as an order of magnitude estimate, if for instance  $B(0) = 10$  G when  $h_{\text{CME}} = 1.2R_{\text{sun}}$  (Fig. 11 from Fan et al. (2018)) then for a CME at  $3 R_{\text{sun}}$  the magnetic field is  $B(h) = B(0)(1.2/3)^2 = 1.6$  G. One can use the same empirical relationship to rescale the field at higher/lower altitudes if required.

### 5.2. Magnetic Sensitivity and the Simulated Hanle Diagrams

While the VL signal is insensitive to the magnetic field, the linear polarization of D<sub>3</sub> can be modified by the magnetic field due to the Hanle and Zeeman signals. In Figure 5 we show the dependence of the total fractional linear



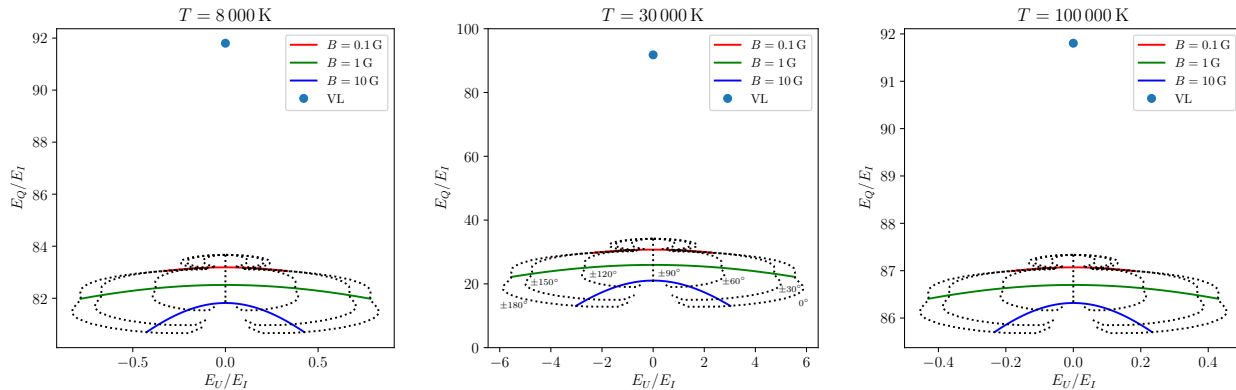


**Figure 6.** Polarization (or Hanle) diagrams of the VL+D<sub>3</sub> signal for three different plasma temperatures, height  $h = 1.6 \times 10^6$  km, and  $p = 0.1$  dyn cm<sup>-2</sup>. The solid lines correspond to the magnetic field of a fixed strength and changing azimuth  $\chi_B$  (indicated in the central panel). The dotted lines show the signals for fixed magnetic field azimuth and varying strength. The signal of VL, i.e., neglecting the D<sub>3</sub> contribution, is shown by the blue dot on the top of the panels.

polarization signals of the VL+D<sub>3</sub> on the magnetic field strength. Even a very weak magnetic field ( $B < 1$  G) causes partial relaxation of the quantum coherence in the  $2p^3P$  and  $2s^3S$  levels leading to the lower-level Hanle effect, hence to a sensitivity of the polarization signal to sub-G fields (Bommier 1980). At fields of the order of few G, the signal is highly sensitive to the upper-term Hanle effect in  $3d^3D$ . Above  $\approx 6$  G, the  $J$ -level crossings start to occur and the upper term enters the so-called incomplete Paschen-Back effect (see, e.g., Sahal-Brechot 1981). These effects are most obvious in the central panels of Figure 5 where the D<sub>3</sub> line dominates the total signal while in the cooler or hotter plasmas the depolarization and rotation of the polarization vector are less obvious.

The Hanle diagrams shown in Figure 6 further demonstrate the sensitivity of the linear polarization signal to different magnetic field strengths and orientations. It follows that the main impact of the D<sub>3</sub> line is a lowering of the fractional polarization  $E_Q/E_I$  due to relatively high D<sub>3</sub> intensity at temperatures around 30 - 50,000 K. However, for certain combinations of magnetic field strength and orientation, the Hanle effect can leave measurable signatures in the linear polarization signal. For instance, at  $B = 3$  G and  $\chi_B = 0^\circ$ , the polarization vector can be rotated by about  $10^\circ$  with respect to the nearest solar limb, thus providing a measurable positive evidence for the presence of magnetic field. In other cases, depolarization of the Stokes  $Q$  parameter still provides a valuable constraint on the thermal conditions of the CME plasma.

## 6. DISCUSSION AND CONCLUSIONS

In order to detect signatures of the D<sub>3</sub> line emission in the integrated signal from the VL filter of Metis, we must estimate the relative intensities of the line and VL continuum which is due to Thomson scattering on free electrons in the CME core. The core is usually well recognized as a bright flux rope or a patchy prominence-like structure, see e.g. Heinzel et al. (2016) or Floyd & Lamy (2019) (their Figure 1) so that we can neglect other VL contributions due to a CME halo (quiet-corona emission is normally subtracted from images). Our theoretical estimates for a range of plausible CME-core models are given in Table 1 where we can see that the D<sub>3</sub> contribution is non-negligible and in the temperature range between 30,000 and 50,000 K it significantly dominates over the VL one (we discuss this behaviour in Section 3). We know that such temperatures are present inside CME cores, see e.g. Jejić et al. (2017). At 30,000 K, the D<sub>3</sub> line is a factor 5-7 brighter compared to VL. At low temperatures VL signal dominates and at  $10^5$  K the line contribution is less than 10 %.

Normally one cannot infer a dominance of the line emission over the VL continuum just from the fact that the CME core is structured like a cool prominence (see Figure 1 in Floyd & Lamy (2019) and the caption). This is because the CME-core electron densities will produce a similar pattern in VL due to Thomson scattering. However, we can disentangle between these two contributions using linear polarization measurements. Looking at Figure 4 (right panel), we see that for temperatures between say 20,000 and 80,000 K the polarization degree  $E_Q/E_I$  is significantly lower compared to a constant 80 - 90 % polarization which is only due to Thomson scattering. This corresponds to an intensity enhancement (peak) on the left panel of Figure 4 which is due to D<sub>3</sub> emission. Our models can thus, at least

qualitatively, explain the behaviour of LASCO-C2 observations analyzed by Floyd & Lamy (2019). LASCO-C2 orange filter is even wider (540 - 640 nm) than the Metis VL filter, and also contains the D<sub>3</sub> line (in its central part). At least in two cases analyzed by these authors, the detected polarization is surprisingly low compared to expected high-degree polarization due to Thomson scattering alone. The authors thus conclude that this might be due to a presence of the D<sub>3</sub> line and they think about possible depolarization due to Hanle effect. But since we know the brightness of the D<sub>3</sub> line in our models, we see that the line is sometimes very bright and therefore total  $E_Q$  over total  $E_I$  is low even in a non-magnetic case. It is interesting to note that a low polarization was also detected in a CME by Mierla et al. (2011) using the wide-band filter of SECCHI/COR1 coronagraph which contains the hydrogen H $\alpha$  line in its center. Note that this line is typically much brighter in cool prominence structures as compared to D<sub>3</sub>.

At this point we should mention that both Metis as well as LASCO-C2 filters contain Na I doublet red-ward of the D<sub>3</sub> line at 589.16 nm and 589.76 nm (the rest wavelength). These lines are also in emission in prominence-like structures and thus may contaminate the total VL signal. However, as thoroughly discussed in Jeřič et al. (2018), their typical brightness is much lower compared to D<sub>3</sub> line and thus we neglect them in our present analysis.

Based on our estimation of the magnetic-field strength in CMEs, we studied the Hanle effect on D<sub>3</sub> line. Concerning the orientation of the magnetic-field vector in a CME core, we can at least see from numerous observations that the expanding flux-rope top is more or less parallel to the solar limb and this is very favorable for the field detection via the Hanle effect in the D<sub>3</sub> line. Our results are presented and briefly discussed in Section 5. We show that under some conditions it will be possible to diagnose CME magnetic field using the VL channel of Metis. At low temperatures (our models with 8,000 K) and for B around 10 G, the Hanle depolarization is only by about 2 % (similar to quiescent prominences), at 10<sup>5</sup> K it is even lower. But for intermediate temperatures the depolarization amounts to 10 % or more - see polarization diagrams in Figure 6. At 30,000 K we see a significant lowering of polarization degree just due to D<sub>3</sub> brightness plus about 10 % lowering due to 10 G magnetic field. The polarization capabilities of Metis are described in Antonucci et al. (2019) and Fineschi et al. (2020) and in a following paper we plan to perform a more detailed analysis of Metis VL-channel response to magnetic-field and thermal structure of CMEs. In parallel we are studying a diagnostics potential of the Metis Lyman  $\alpha$  channel which can provide an independent information on CME thermal structure. Finally, D<sub>3</sub> line intensity (i.e. Stokes  $I$ ) and broad-band VL polarization will be detected by the SPIICS coronagraph on board of ESA's Proba-3 formation-flight mission and thus a synergy with Metis will be of great interest.

#### ACKNOWLEDGMENTS

Solar Orbiter is the ESA mission towards the Sun launched by NASA on February 10, 2020. Metis is its payload coronagraph developed by the Italian-German-Czech consortium, under the leadership of Italian ASI. The authors acknowledge support from the grants No. 19-17102S and 19-20632S of the Czech Funding Agency and from RVO:67985815 project of the Astronomical Institute of the Czech Academy of Sciences. The Czech contribution to Metis was funded by ESA-PRODEX. S.J. acknowledges the support from the Slovenian Research Agency No. P1-0188. N.L. acknowledges support from the Science and Technology Facilities Council (STFC) Consolidated Grant No. ST/P000533/1.

*Facility:* Solar Orbiter - Metis

#### REFERENCES

- Antonucci, E., Romoli, M., Andretta, V., et al. 2019, arXiv e-prints, arXiv:1911.08462.  
<https://arxiv.org/abs/1911.08462>
- Asensio Ramos, A., Trujillo Bueno, J., & Landi Degl'Innocenti, E. 2008, ApJ, 683, 542,  
 doi: 10.1086/589433
- Bommier, V. 1977, Thèse de 3ème cycle, Université de Paris VI
- . 1980, A&A, 87, 109
- Cox, A. N. 2000, Allen's astrophysical quantities
- Dal Lago, A., Schwenn, R., & Gonzalez, W. D. 2003, Advances in Space Research, 32, 2637,  
 doi: 10.1016/j.asr.2003.03.012
- Dolei, S., Bemporad, A., & Spadaro, D. 2014, A&A, 562, A74, doi: 10.1051/0004-6361/201321041
- Fan, Y., Gibson, S., & Tomczyk, S. 2018, ApJ, 866, 57,  
 doi: 10.3847/1538-4357/aadd0e

- Fineschi, S., Naletto, G., Romoli, M., et al. 2020, *Experimental Astronomy*, doi: [10.1007/s10686-020-09662-z](https://doi.org/10.1007/s10686-020-09662-z)
- Floyd, O., & Lamy, P. 2019, *SoPh*, 294, 168, doi: [10.1007/s11207-019-1553-0](https://doi.org/10.1007/s11207-019-1553-0)
- Heasley, J. N., Mihalas, D., & Poland, A. I. 1974, *ApJ*, 192, 181, doi: [10.1086/153049](https://doi.org/10.1086/153049)
- Heinzel, P., Susino, R., Jejčič, S., Bemporad, A., & Anzer, U. 2016, *A&A*, 589, A128, doi: [10.1051/0004-6361/201527421](https://doi.org/10.1051/0004-6361/201527421)
- Jejčič, S., Heinzel, P., Labrosse, N., et al. 2018, *SoPh*, 293, 33, doi: [10.1007/s11207-018-1251-3](https://doi.org/10.1007/s11207-018-1251-3)
- Jejčič, S., Susino, R., Heinzel, P., et al. 2017, *A&A*, 607, A80, doi: [10.1051/0004-6361/201731364](https://doi.org/10.1051/0004-6361/201731364)
- Kuridze, D., Mathioudakis, M., Morgan, H., et al. 2019, *ApJ*, 874, 126, doi: [10.3847/1538-4357/ab08e9](https://doi.org/10.3847/1538-4357/ab08e9)
- Labrosse, N. 2015, *Astrophysics and Space Science Library*, Vol. 415, *Derivation of the Major Properties of Prominences Using NLTE Modelling*, ed. J.-C. Vial & O. Engvold, 131, doi: [10.1007/978-3-319-10416-4\\_6](https://doi.org/10.1007/978-3-319-10416-4_6)
- Labrosse, N., & Gouttebroze, P. 2001, *A&A*, 380, 323, doi: [10.1051/0004-6361:20011395](https://doi.org/10.1051/0004-6361:20011395)
- . 2004, *ApJ*, 617, 614, doi: [10.1086/425168](https://doi.org/10.1086/425168)
- Labrosse, N., Heinzel, P., Vial, J. C., et al. 2010, *SSRv*, 151, 243, doi: [10.1007/s11214-010-9630-6](https://doi.org/10.1007/s11214-010-9630-6)
- Lamy, P. L., Vivès, S., Curdt, W., et al. 2017, in *Society of Photo-Optical Instrumentation Engineers (SPIE) Conference Series*, Vol. 10565, *Proc. SPIE*, 105650T, doi: [10.1117/12.2309188](https://doi.org/10.1117/12.2309188)
- Landi Degl’Innocenti, E., & Landolfi, M. 2004, *Polarization in Spectral Lines*, Vol. 307, doi: [10.1007/978-1-4020-2415-3](https://doi.org/10.1007/978-1-4020-2415-3)
- López Ariste, A. 2015, *Astrophysics and Space Science Library*, Vol. 415, *Magnetometry of Prominences*, ed. J.-C. Vial & O. Engvold, 179, doi: [10.1007/978-3-319-10416-4\\_8](https://doi.org/10.1007/978-3-319-10416-4_8)
- Mierla, M., Chifu, I., Inhester, B., Rodriguez, L., & Zhukov, A. 2011, *A&A*, 530, L1, doi: [10.1051/0004-6361/201016295](https://doi.org/10.1051/0004-6361/201016295)
- Mihalas, D., & Stone, M. E. 1968, *ApJ*, 151, 293, doi: [10.1086/149437](https://doi.org/10.1086/149437)
- Sahal-Brechot, S. 1981, *SSRv*, 29, 391
- Sahal-Brechot, S., Bommier, V., & Leroy, J. L. 1977, *A&A*, 59, 223
- Susino, R., Bemporad, A., Jejčič, S., & Heinzel, P. 2018, *A&A*, 617, A21, doi: [10.1051/0004-6361/201832792](https://doi.org/10.1051/0004-6361/201832792)
- Trujillo Bueno, J., & Shchukina, N. 2009, *ApJ*, 694, 1364